Supporting Information for

The Physical and Electronic Properties of Metal-Organic Frameworks Containing Dipyridylthiazolo[5,4-*d*]thiazole

Felix J. Rizzuto,[bc] Shyam C. Pal,[d] Eleanor R. Kearns,[ab] Carol Hua,[e] Marcello B. Solomon,[ab] Patrick W. Doheny,[b] Thomas B. Faust,[b] Cameron J. Kepert,[b]* Madhab C. Das,[d]* Deanna M. D'Alessandro.[ac]*

[a] School of Chemical and Biomolecular Engineering, Faculty of Engineering, The University of Sydney, New South Wales, Australia 2006
[b] School of Chemistry, The University of Sydney, New South Wales 2006, Australia
[c] School of Chemistry, The University of New South Wales 2052, Australia
[d] Department of Chemistry, IIT Kharagpur, Kharagpur – 721302, West Bengal, India
[e] School of Chemistry, The University of Melbourne, Parkville, Victoria 3010, Australia

* *Corresponding Authors: mcdas@chem.iitgp.ac.in; deanna.dalessandro@sydney.edu.au*

Table of Contents

Materials and Methods

Materials

Unless otherwise stated, all reagents and solvents employed were commercially available and used as received without further purification. For electrochemical experiments, acetonitrile and chloroform were dried over CaH_2, then distilled under N_2. Tetra-*n*-butyl ammonium hexafluorophosphate ([*n*-Bu_4N]PF_6) was recrystallised three times from absolute ethanol before being dried *in vacuo*. 2,5-Di(4-pyridyl)thiazolo[5,4-*d*]thiazole (**L**) was synthesised by a literature procedure, and the experimental data matched that previously reported.[1]

Methods

Powder X-ray Diffraction (PXRD): PXRD data were obtained using a Bruker D8 Advance diffractometer or PANanalytical X'Pert PRO Multi-Purpose Diffractometer producing Cu-K_α (λ = 1.5406 Å) radiation, equipped with a solid-state PIXcel detector. Flat plate samples were collected at a rate of 0.028° min^{-1} over the interval $5 \leq 2\theta \leq 50°$ with a step size of 0.013°. Capillaries were analysed using the same conditions. Air sensitive samples were loaded into glass capillaries under an inert Ar atmosphere and capped with silicone grease prior to flame sealing. Lattice parameters were determined using the Le Bail intensity extraction method, which was performed in GSAS[2] using EXPGUI.[3] Powder pattern simulations from SCXRD data were generated using the program Mercury 3.0.[4]

Variable temperature PXRD data were collected over the range 298-600 K using an Oxford Cryosystems 700 N_2 cryostream. Data were collected at either 5 or 20 K intervals, using a heating rate of 360 K h^{-1}. A 5 min settling period was used to allow the cryostream and sample to equilibrate.

Elemental Analysis: Elemental analyses (C, H, N, S) were performed on **2-Zn** and **3-Zn** on an Elementar Vario Micro Cube elemental analyser. Elemental analyses of **1-Zn**, **1-Mn** and **1-Cu** were collected by Dr Remi Rouquette at the Chemical Analysis Facility – Elemental Analysis Service in the Department of Chemistry and Biomolecular Science at Macquarie University, Australia.

Thermogravimetric Analysis (TGA): TGA data for **1-Zn**, **1-Mn** and **1-Cu** were collected on a TA Instruments' Hi-Res TGA 2950 Thermogravimetric Analyser. After equilibrating to 298 K and holding isothermal for 20 min, each sample was heated to 1000 K at a ramp rate of 2 K min^{-1} under a constant

flow of N_2 (0.1 L min^{-1}). Data for **2-Zn** and **3-Zn** were collected on a Netzsch TG 209 *F3* Tarsus (Netzsch). The sample was heated from room temperature to 1000 K at a ramp rate of 5 K min^{-1} under a constant flow of N_2.

Ultraviolet-Visible-Near Infrared (UV-Vis-NIR) Spectroscopy: Solid-state UV-Vis-NIR spectroscopy was performed using a CARY 5000 spectrometer with a Praying Mantis attachment over the range 5000-50000 cm^{-1}. Air-sensitive samples were loaded into an air-tight cell under an inert atmosphere. A baseline correction was undertaken with dry, finely ground $BaSO_4$.

Fourier-Transformed Infrared (FT-IR) Spectroscopy: FT-IR spectroscopy was performed using a Perkin-Elmer RX1 spectrophotometer over the range 400-4000 cm^{-1}.

Cyclic voltammetry (CV): Solution- and solid-state CV were performed using a BASi Epsilon Electrochemical Analyser with ferrocene/ferrocenium (Fc/Fc^+) used as an internal reference standard. Measurements were conducted under an inert Ar atmosphere using a conventional three-electrode cell: a glassy carbon working electrode (1.5 mm diameter), a Pt wire counter electrode, and a Ag/Ag^+ *quasi*-reference electrode. A 0.1 M tetrabutylammonium hexafluorophosphate ([*n*-$Bu_4N]PF_6$) electrolyte in acetonitrile or chloroform was employed, which was purged with Ar gas prior to experiments. Scan rate-dependence studies were performed in the range of 25-200 mV s^{-1}. For the solution state CV, the analyte was dissolved in the electrolyte, while for solid-state CV, the material was mechanically immobilised onto the surface of the working electrode prior to measurement. Following solid-state experiments, the electrolyte was checked for the presence of electroactive material which may have leached out of the framework material.

Solid-State Visible-Near Infrared (Vis-NIR) Spectroelectrochemistry (SEC): Vis-NIR data were collected using a CARY5000 spectrometer equipped with a Harrick OmniDiff Probe attachment. Diffuse reflectance spectra of the electrogenerated species were collected *in situ* using a custom-made three-electrode cell using over the range 5000-25000 cm^{-1}.[5] The Teflon electrochemical cell comprised of a central reservoir, connected to two side arms, filled to the top of the central chamber with an electrolyte solution containing [*n*-$Bu_4N]PF_6$ (0.1 M) in acetonitrile. The separate side arms (separately accommodating a Pt wire auxiliary electrode, and a Ag/Ag^+ wire *quasi*-reference electrode, respectively), both protruded into the central compartment harbouring the electrolyte without contacting each other. The sample of interest was immobilised onto an Indium-Tin-Oxide (ITO) coated quartz slide working electrode (0.1 mm width) using a thin strip of Teflon tape, on which

the baseline scan was collected. The electrode was inverted over the central compartment to enable contact between the sample and electrolyte, fixed with adhesive tape, and the circuit completed with conductive copper tape. Potentials applied to the cell were controlled using an eDAQ e-corder 410 potentiostat. Continuous scans of the sample were undertaken at a potential of 0 V until spectral equilibration was achieved. A cathodic potential was then manually applied incrementally prior to the collection of spectra. Spectra were reported as the Kubelka-Munk transformation.

Structural and Electrochemical Characterisation of L

Table S1: Crystal data and structure refinement for **L-α** and **L-β**

Identification code	**L-α**	**L-β**
Empirical formula	$C_{14}H_8N_4S_2$	$C_{14}H_8N_4S_2$
Formula weight	296.36	296.36
Temperature / K	150(2)	150(2)
Crystal system	monoclinic	monoclinic
Space group	$P2_1/c$	$P2_1/c$
a / Å	8.4275(6)	15.6685(7)
b / Å	6.3040(4)	3.78420(10)
c / Å	11.7480(7)	10.8705(5)
α / °	90	90
β / °	93.544(6)	108.658(5)
γ / °	90	90
Volume / Å^3	622.94(7)	610.67(4)
Z	2	2
ρ_{calc} / mg mm^{-3}	1.580	1.612
μ / mm^{-1}	0.420	3.896
F(000)	304.0	304.0
Crystal size / mm^3	0.37 × 0.13 × 0.11	0.35 × 0.11 × 0.07
Radiation	MoKα (λ = 0.71073 Å)	CuKα (λ = 1.54178 Å)
2Θ range for data collection	6.96 to 60.12°	11.92 to 152.34°
Index ranges	−11 ≤ h ≤ 11, −8 ≤ k ≤ 8, 16 ≤ l ≤ 14	−19 ≤ h ≤ 19, −4 ≤ k ≤ 3, -13 ≤ l ≤ 11
Reflections collected	5958	4197
Independent reflections	1645 [R_{int} = 0.0395, R_{sigma} = 0.0411]	1267 [R_{int} = 0.0172, R_{sigma} = 0.0146]
Data/restraints/parameters	1645/18/91	1267/0/91
Goodness-of-fit on F^2	1.077	1.093
Final R indices [I≥2σ(I)]	R_1 = 0.0418, wR_2 = 0.1004	R_1 = 0.0345, wR_2 = 0.0947
Final R indices [all data]	R_1 = 0.0531, wR_2 = 0.1071	R_1 = 0.0353, wR_2 = 0.0952
Largest diff. peak/hole / e Å^{-3}	0.43/−0.23	0.42/−0.31

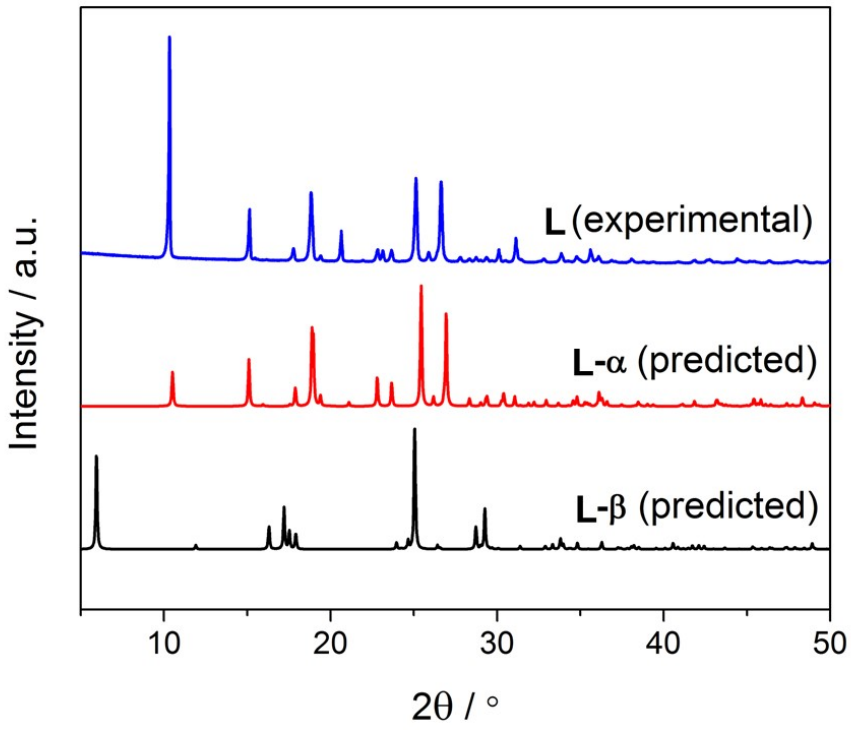

Figure S1: Comparison of predicted PXRD patterns of **L-α** (red) and **L-β** (black) obtained by SCXRD (150 K) with the bulk synthesis of **L** (blue; 298 K).

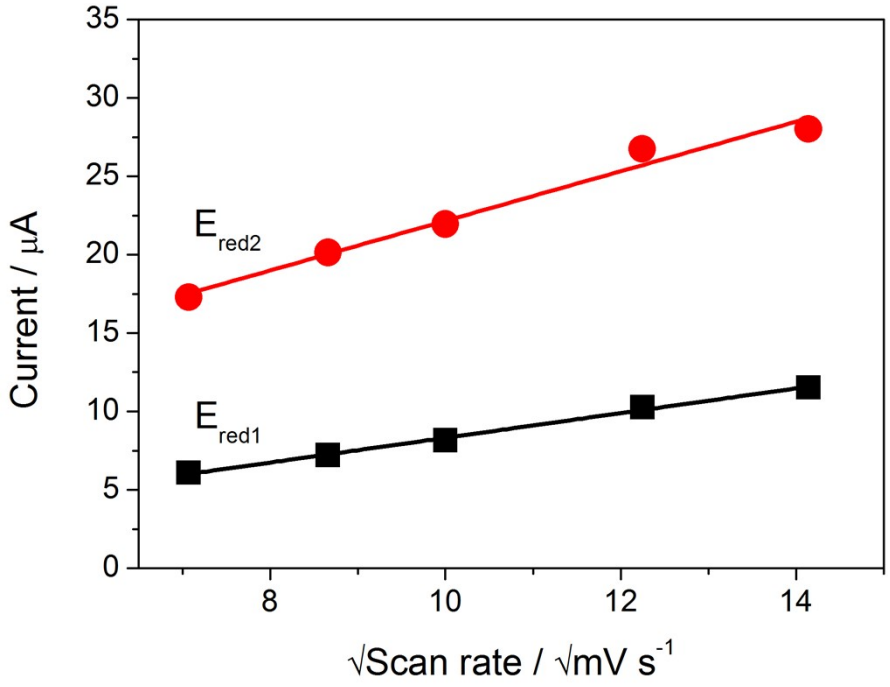

Figure S2: Comparison of the current of the first (black) and second (red) reduction processes as a function of the square root of the scan rate, according to the Randles-Sevcik equation.

Synthesis of MOFs Containing L

Variation of Metal Node

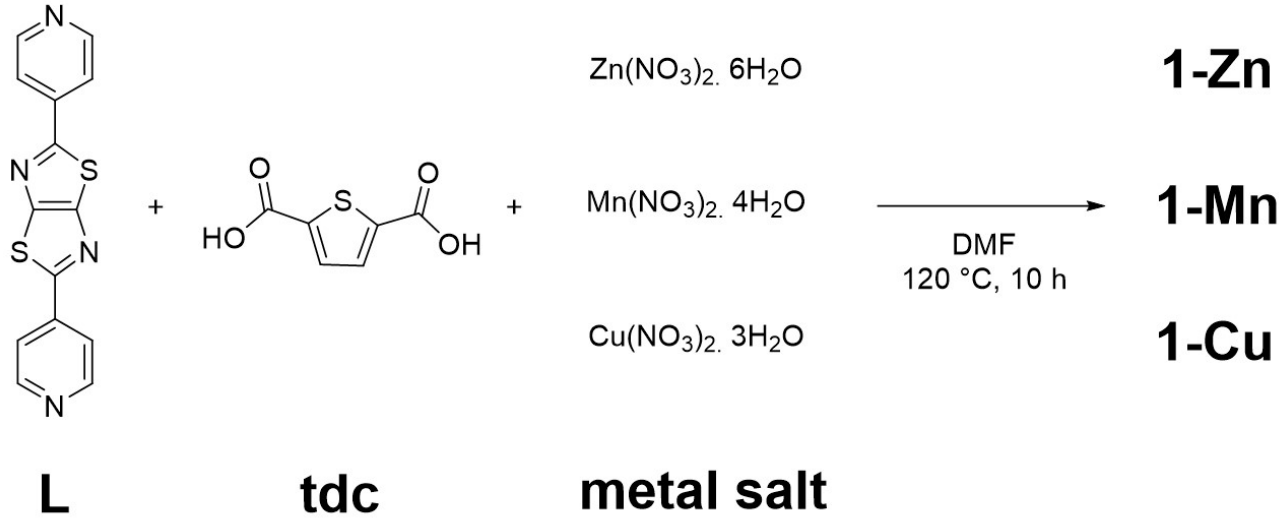

Scheme S1: The synthesis of **DPTzTz** MOFs, varying the metal node.

$[M_2(tdc)_2(L)_2]\cdot 2DMF$ (M = Zn, Cu, Mn) (tdc = 2,5-thiophenedicarboxylic acid). $M(NO_3)_2\cdot xH_2O$ (120 mg, 0.40 mmol), tdc (69 mg, 0.40 mmol) and **L** (60 mg, 0.20 mmol) were heated in DMF (40 mL) at 393 K for 10 h. The precipitate was filtered hot, washed with DMF and dried *in vacuo* to afford $[M_2(tdc)_2(\mathbf{L})_2]\cdot 2DMF$ (M = Zn: light yellow, 120 mg, 97%, **1-Zn**; M = Mn: bright yellow, 64 mg, 54%, **1-Mn**; M = Cu: light green, 61 mg, 51%, **1-Cu**).

1-Zn: Elemental analysis (%) calculated for $C_{40}H_{22}N_8O_8S_6Zn_2$: C 45.08, H 2.08, N 10.51, S 18.05, found: C 45.02, H 2.63, N 10.13, S 17.82. **FT-IR(cm^{-1})**: 1676(s), 1587(s), 1525(m), 1447(w), 1365(s), 1212(w), 1090(w), 1065(w), 1028(w), 1013(w) 813(m), 773(s), 703(s), 666(w), 618(m), 507(m).

1-Mn: Elemental analysis (%) calculated for $C_{40}H_{22}N_8O_8S_6Mn_2$: C 45.98, H 2.12, N 10.72, S 18.41, found: C 46.16, H 2.32, N 11.08, S 18.56. **FT-IR(cm^{-1})**: 3340(br), 1677(s), 1584(w), 1539(s), 1510(s), 1488(s), 1369(s), 1340(s), 1316(w), 1216(w), 1125(w), 1088(w), 1063(w), 1042(w), 1026(w), 1009(w), 814(w), 773(s), 699(w), 678(w), 666(w), 616(w), 538(w), 500(w).

1-Cu: Elemental analysis (%) calculated for $C_{40}H_{22}N_8O_8S_6Cu_2$: C 45.23, H 2.09, N 10.55, S 18.11, found: C 45.16, H 2.39, N 10.44, S 17.74. **FT-IR(cm^{-1})**: 3071(br), 1676(s), 1601(s), 1561(w), 1525(w), 1443(w), 1388(s), 1351(s), 1327(s), 1216(w), 1088(w), 1064(w), 1037(w), 1021(w), 937(w), 838(w), 823 (w), 802 (w), 768(s), 706(w), 686(w), 666(w), 618(w), 566(w), 550(w), 506(w).

Variation of Co-Ligand

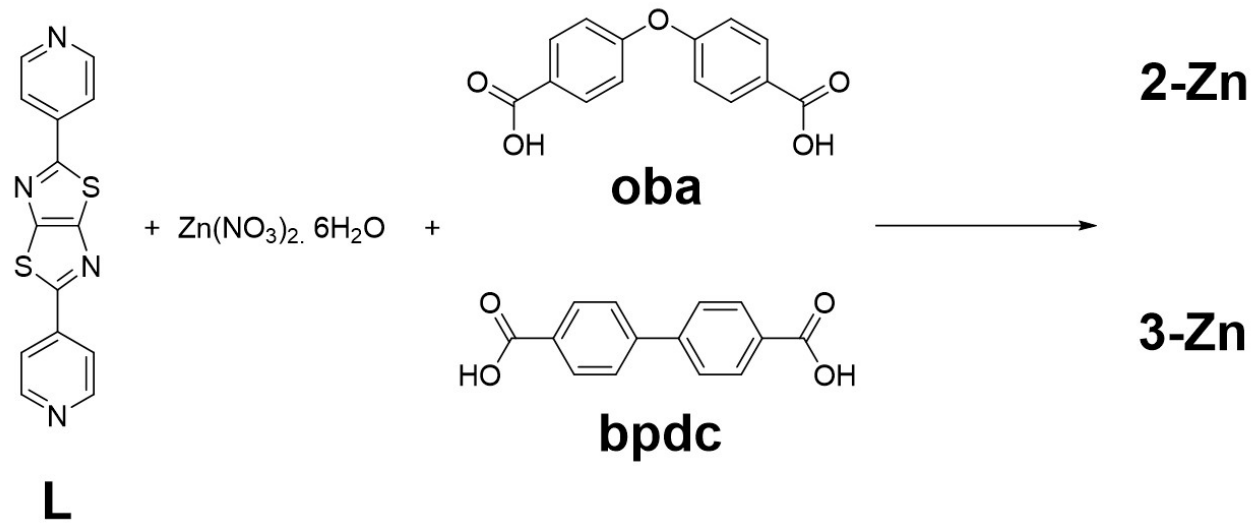

Scheme S2: The synthesis of **DPTzTz** MOFs, varying the co-ligand.

Synthesis of [Zn(oba)(L)]·DMF·H_2O (2-Zn). $Zn(NO_3)_2{\cdot}6H_2O$ (15 mg, 0.05 mmol), 4,4´-oxy*bis*benzene dicarboxylic acid (oba) (10 mg, 0.04 mmol) and **L** (8 mg, 0.03 mmol) were dissolved in a solution of DMF/deionised H_2O ((4:1), 2.5 mL). The solution was stirred at room temperature for 30 min before heating at 373 K for 2 d. The sample was slowly cooled to room temperature over 10 h. Yellow block-shaped crystals were collected by filtration, washed with DMF to afford [Zn(oba)(**L**)]·DMF·H_2O (**2-Zn**), which was stored in fresh mother liquor (Yield: 20 mg (64% based on $Zn(NO_3)_2{\cdot}6H_2O$)).

Elemental analysis (%) calculated for $C_{31}H_{25}N_5O_7S_2Zn$: C 52.50, H 3.55, N 9.87, S 9.04, found: C 52.23, H 3.45, N 9.82, S 9.33. **FT-IR(cm^{-1}):** 3404(b), 3066(w), 2935(w), 2876(w) 1655(s), 1632(s), 1608(s), 1550(w), 1498(w), 1439(w), 1388(s), 1326(w), 1255(w), 768(s), 679(m), 662(m).

Synthesis of $[Zn_2(bpdc)_2(L)_2]{\cdot}L$. $Zn(NO_3)_2{\cdot}6H_2O$ (15 mg, 0.05 mmol), biphenyl-4,4´-dicarboxylic acid (bpdc) (10 mg, 0.04 mmol) and **L** (8 mg, 0.027 mmol) were dissolved in a solution of DMF/deionised H_2O ((4:1), 2.5 mL). The solution was stirred at room temperature for 30 min before heating at 373 K for 2 d. The sample was slowly cooled to room temperature over 12 h. Yellow block shaped crystals were collected by filtration, washed with DMF to afford **$[Zn_2(bpdc)_2(L)_2]{\cdot}L$** (**3-Zn**), which was stored in fresh mother liquor (Yield: 20 mg (39% based on $Zn(NO_3)_2{\cdot}6H_2O$)).

Elemental analysis (%) calculated for $C_{70}H_{40}N_{12}O_8S_6Zn_2$: C 56.03, H 2.68, N 11.20, S 12.82, found; C 55.92, H 2.61, N 11.45, S 12.78. **FT-IR(cm^{-1}):** 3395(b), 3381(w), 3298(w), 3103(w), 3077(w), 3061(w), 3044(w), 1672(s), 1634(s), 1610(m), 1591(s), 1498(w), 1442(m), 1392(s), 1225(m), 694(s)

MOF Crystallography and Structural Studies

Data Collection

1-Zn: Single crystals of **1-Zn** were obtained by scaling down the bulk synthesis by one sixth, using DMF (10 mL) and heating at 393 K for 48 h. They were grown in a sealed 21 mL glass scintillation vial, which was heated in an aluminium-lined incubation block with no agitation. Diffraction data for **1-Zn** were collected on an Agilent Technologies SuperNova diffractometer employing Cu-K_α (λ = 1.54178 Å) radiation. An Oxford Cryosystems 700 Plus cryostream attachment produced a continuous stream of N_2 at 150 K. Yellow block crystals were coated in a thin film of paratone-*N* oil and mounted on a mohair fibre affixed to a goniometer head. Data reduction, integration and absorption corrections were performed using the Agilent Technologies CrysAlisPro[6] software (version 1.171.35.8). Subsequent computations were performed with the WINGX[7] and Olex2[8] graphical user interfaces. The structure for **1-Zn** was solved by direct methods using SHELXS-97,[9] and refined within SHELXL-97[9] using the full-matrix least-squares on F^2 method. Non-hydrogen atoms were refined anisotropically and hydrogen atoms were geometrically fixed using a riding atom model. Guest-accessible pore volumes were calculated in PLATON,[10] and geometric parameters were extracted in Mercury 3.0.[4] Structure illustrations were produced using X-Seed.[11]

2-Zn and 3-Zn: Single, yellow, block-shaped crystals of **2-Zn** and **3-Zn** suitable for single crystal X-ray diffraction were obtained directly from the bulk synthesis. They were grown in a sealed 15 mL glass vial, which was heated in an oven. Diffraction data for **2-Zn** and **3-Zn** were collected on a Bruker SMART APEX II CCD diffractometer employing graphite-monochromated Mo-K_α radiation (λ = 0.71073 Å). Yellow block crystals were coated in a thin film of paratone-*N* oil, mounted on a glass fibre and secured using epoxy resin. Single crystal X-ray data were collected at 298 K for **2-Zn** and 100 K for **3-Zn**. The linear absorption coefficients, scattering factors for the atoms, and the anomalous dispersion corrections were taken from International Tables for X-ray Crystallography. Data reduction and integration were performed with SAINT[12] software. Empirical absorption correction was applied to the collected reflections with SADABS using XPREP.[13] The structure was solved by direct methods using SHELXTL,[14] and refined within SHELXL-2014[15] using the full-matrix least-squares on F^2 method. Non-hydrogen atoms were refined anisotropically and hydrogen atoms were geometrically fixed using a riding atom model. Guest-accessible pore volumes were calculated in PLATON.[10]

Table S2: Crystal data and structure refinement for **1-Zn, 2-Zn** and **3-Zn**

Identification code	**1-Zn**	**2-Zn**	**3-Zn**
Empirical formula	$C_{46}H_{34}N_{10}O_{10}S_6Zn_2$	$C_{28}H_{16}N_4O_5S_2Zn$	$C_{70}H_{40}N_{12}O_8S_6Zn_2$
Formula weight	1209.93	617.96	1500.28
Temperature / K	150(2)	298(2)	100(2)
Crystal system	monoclinic	monoclinic	triclinic
Space group	$P2_1/c$	$C2/c$	$P\bar{1}$
a / Å	17.1947(2)	32.53(2)	14.728(7)
b / Å	18.5446(2)	8.664(3)	15.36(5)
c / Å	15.7154(2)	22.10(2)	15.369(8)
α / °	90	90	93.63(7)
β / °	100.9740(10)	96.56(2)	113.88(4)
γ / °	90	90	91.64(5)
Volume / Å^3	4919.51(10)	6188(7)	3167(11)
Z	4	8	2
ρ_{calc} / mg mm^{-3}	1.634	1.327	1.5763
m / mm^{-1}	4.173	0.964	1.025
F(000)	2464.0	2512.0	1528
Crystal size / mm^3	0.44 × 0.18 × 0.09	0.15 × 0.12 × 0.11	0.14 × 0.09 × 0.07
Radiation	CuKα (λ = 1.54178 Å)	MoKα (λ = 0.7107 Å)	MoKα (λ = 0.7107 Å)
2θ range for data collection	7.08 to 151.86°	2.34 to 26.03°	2.91 to 27.20°
Index ranges	−21 ≤ h ≤ 21, −23 ≤ k ≤ 23, −19 ≤ l ≤ 19	−36 ≤ h ≤ 38, −10 ≤ k ≤ 10, −25 ≤ l ≤ 29	−18 ≤ h ≤ 18, −19 ≤ k ≤ 16, −19 ≤ l ≤ 19
Reflections collected	90347	5310	13748
Independent reflections	10214 [R_{int} = 0.0483, R_{sigma} = 0.0254]	4599 [R_{int} = 0.0647, R_{sigma} = 0.0432]	12243 [R_{int} = 0.0352, R_{sigma} = 0.0488]
Data/restraints/parameters	10207/394/667	5310/0/361	13748/
Goodness-of-fit on F^2	1.076	1.058	1.205
Final R indices [I≥2σ(I)]	R_1 = 0.0730, wR_2 = 0.1756	R_1 = 0.0316, wR_2 = 0.0838	R_1 = 0.0913 wR_2 = 0.2451
Final R indices [all data]	R_1 = 0.0819, wR_2 = 0.1798	R_1 = 0.0367, wR_2 = 0.0859	R_1 = 0.0980 wR_2 = 0.2485
Largest diff. peak/hole / e Å^{-3}	2.57/−0.87	0.261/−0.198	0.099/−0.987

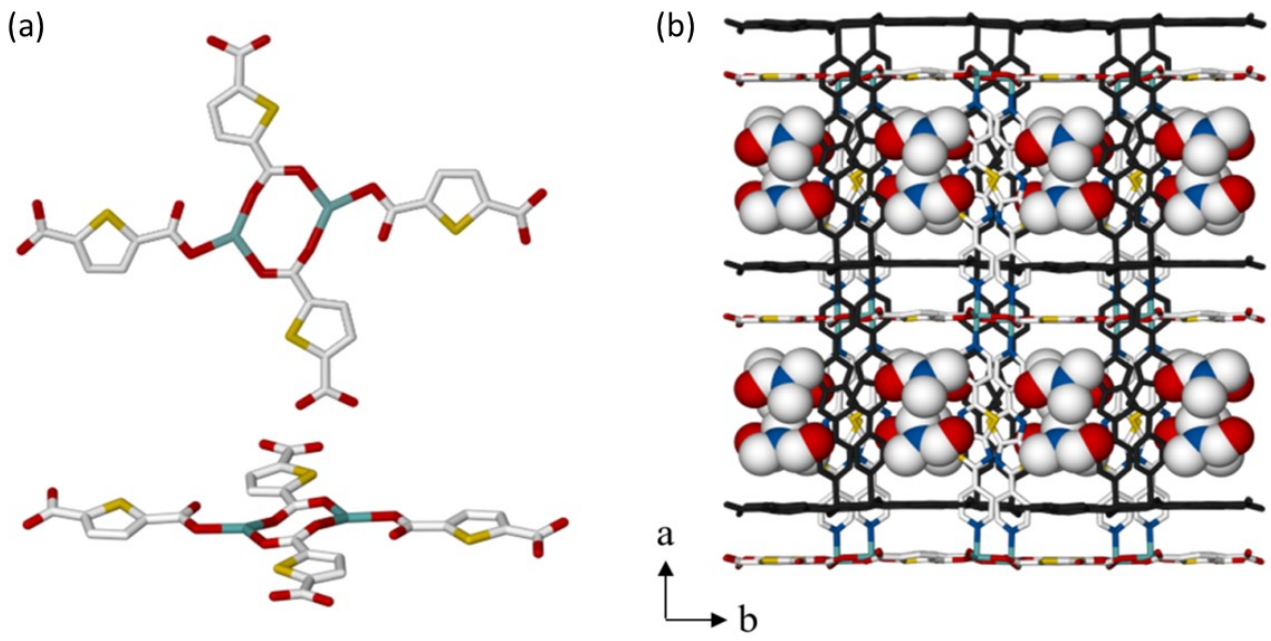

Figure S3: The crystal structure of **1-Zn**. **(a)** The Zn^{II} dimer, showing the connectivity and 'puckering' of the metal ions, and the layering of the sheets, and **(b) 1-Zn** viewed along the *c*-axis (interpenetrated layer shown in black, DMF in the pores shown as van der Waals radii representations). Zn – cyan, C – grey, O – red, N – blue, S – yellow). Hydrogen atoms are omitted for clarity.

Table S3: Selected bond lengths and angles for **1-Zn**

Bond Length	Length (Å)	Bond Angle	Angle (°)
Zn1−O4	2.022(3)	O4−Zn1− N1	89.92(15)
Zn1−O6	2.019(3)	O4−Zn1 −N4	93.71(15)
Zn1−O7	2.013(4)	O6−Zn1 −N1	85.08(15)
Zn1−N1	2.165(4)	O6−Zn1− N4	89.35(16)
Zn1−N4	2.150(4)	O6−Zn1− O4	120.56(14)
Zn2−O1	2.033(4)	O7−Zn1 −N1	89.32(16)
Zn2−O3	2.024(3)	O7−Zn1− N4	94.21(16)
Zn2−O5	2.019(3)	O7−Zn1 −O4	100.96(15)
Zn2−N5	2.139(4)	O7−Zn1 −O6	138.02(15)
Zn2− N8	2.185(4)	N4−Zn1− N1	174.36(17)
		O1−Zn2 −N5	94.22(15)
		O1−Zn2 −N8	89.20(16)
		O3−Zn2− N5	90.76(15)
		O3−Zn2 −N8	85.71(16)
		O3−Zn2 −O1	140.36(15)
		O5−Zn2 −N8	87.68(16)
		O5−Zn2− O1	100.77(15)
		O5−Zn2 −O3	118.22(15)
		N5−Zn2 −N8	176.31(16)

Table S4: Selected non-bonding bonding interactions for **1-Zn**. **D** represents the hydrogen bond donor, **H** represents hydrogen and **A** represents the hydrogen bond acceptor.

D H···A	d(H···A) (Å)	D(D···A) (Å)	< DHA (°)
C11 H11···O60	2.308(0)	3.194(0)	154.99(1)
C28 H28···O50	2.351(0)	3.211(0)	150.16(1)
C61 H61c···N3	2.609(0)	3.553(0)	161.86 (1)
C28 H28···O50	2.351(0)	3.211(0)	150.16(1)
C2 H2···O7	2.496(0)	3.177(0)	128.71(1)
C12 H12···O4	2.525	3.099	119.12(2)

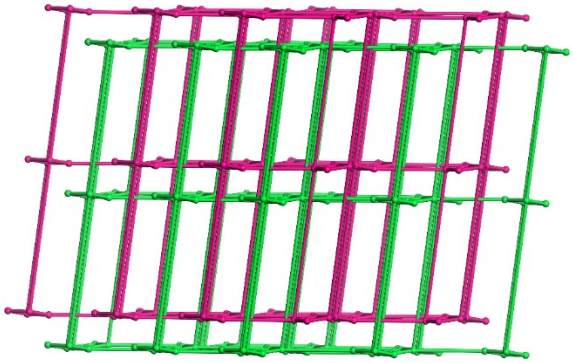

Figure S4: Representation of **1-Zn** showing the network layer with ***sqc*** topology. Green and pink represent the two interpenetrated nets.

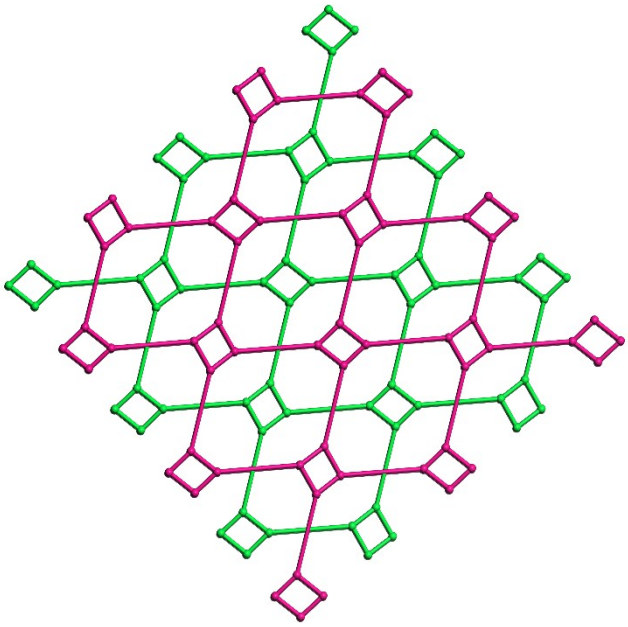

Figure S5: Representation of the 2D layered network of **1-Zn**. Green and pink represent the two interpenetrated nets.

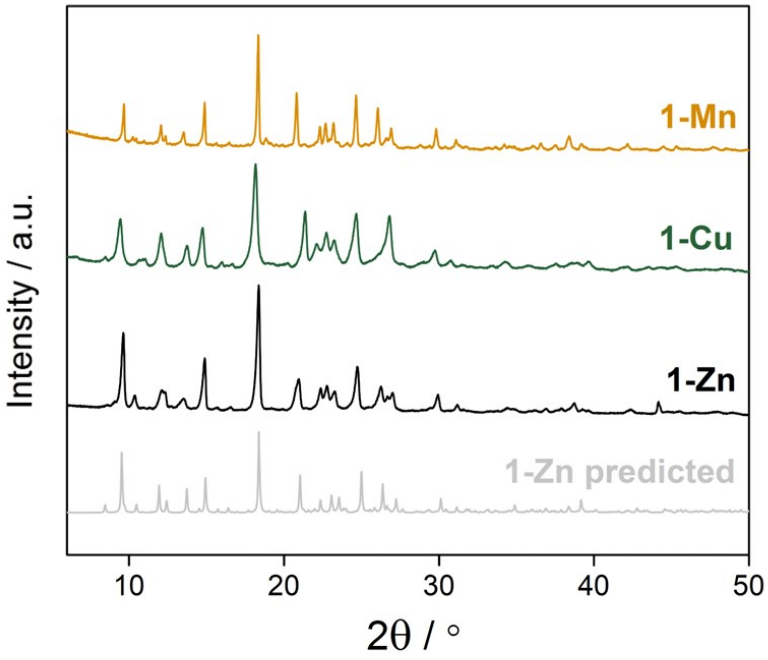

Figure S6: PXRD patterns of **1-Zn** simulated from SCXRD (light grey), experimental **1-Zn** (black), **1-Cu** (green) and **1-Mn** (yellow). The similarity of all three patterns demonstrates the synthesis of an isostructural and phase pure series.

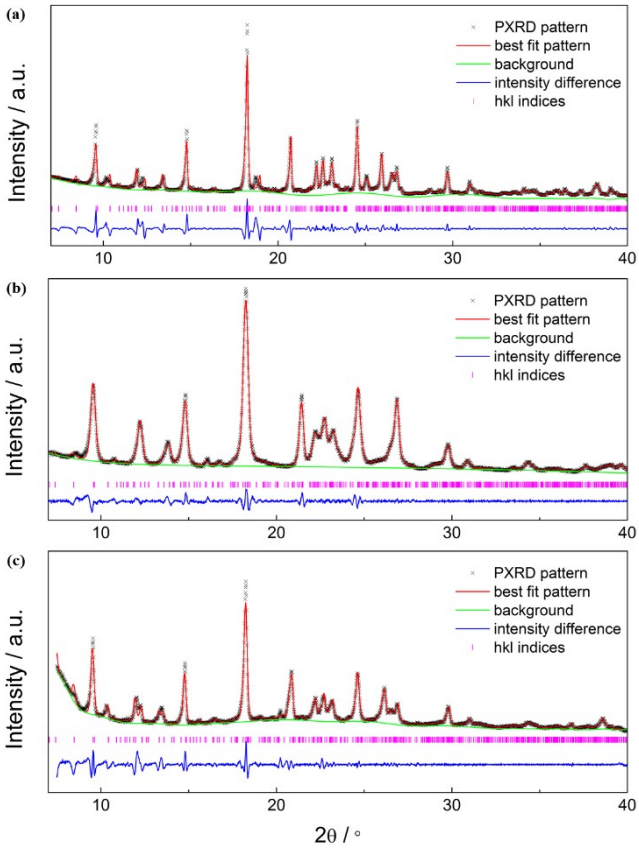

Figure S7: Le Bail extractions of **(a) 1-Mn**, **(b) 1-Cu** and **(c) 1-Zn**.

Table S5: Monoclinic unit cell parameters obtained from Le Bail extractions on PXRD patterns collected for **1-Zn**, **1-Cu** and **1-Mn** at 298 K, compared to SCXRD data collected for **1-Zn** at 150 K.

Framework	*a* / Å	*b* / Å	*c* / Å	*β* / º
1-Zn (SCXRD)	17.1947(2)	18.5446(2)	15.7154(2)	100.986(3)
1-Zn	17.2540(3)	18.5506(7)	15.7604(2)	100.323(13)
1-Cu	17.2773(3)	18.4503(1)	15.9516(1)	100.415(4)
1-Mn	17.2427(6)	18.4723(4)	15.7994(7)	100.987(12)

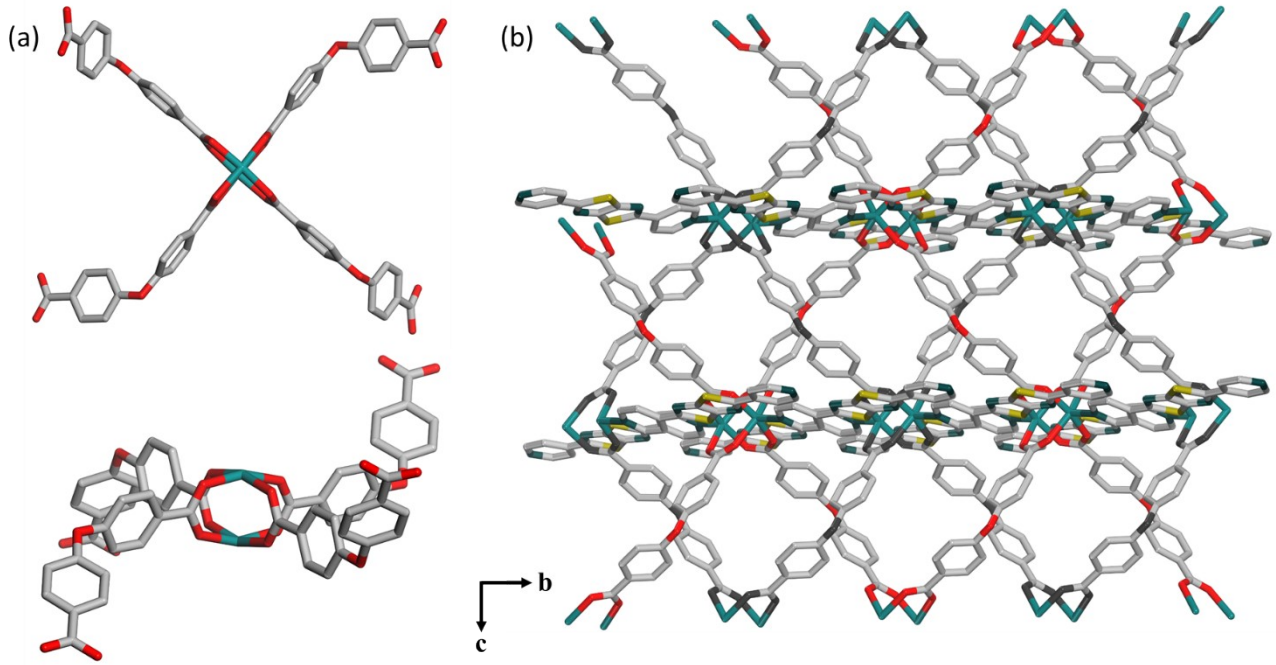

Figure S8: The crystal structure of **2-Zn**. **(a)** The Zn^{II} dimer showing the paddlewheel connectivity. **(b)** **2-Zn** viewed along the a-axis. Zn – cyan, C – grey, O – red, N – blue, S – yellow). Hydrogen atoms are omitted for clarity.

Table S6: Selected bond lengths and angles for **2-Zn**.

Bond Length	Length (Å)	Bond Angle	Angle (°)
Zn1–O1	2.008(3)	O1–Zn1–O2	159.85(7)
Zn1–O2	2.013(3)	O1–Zn1–O3	90.19(5)
Zn1–O3	2.029(3)	O1–Zn1–O4	87.48(16)
Zn1–O4	2.018(3)	O1–Zn1–N1	99.41(12)
Zn1–N1	2.021(3)	O2–Zn1–O3	85.88(16)
Zn1–Zn1	2.900(3)	O2–Zn1–O4	89.49(15)
		O2–Zn1–N1	100.72(12)
		O3–Zn1–O4	159.97(7)
		O3–Zn1–N1	98.94(12)

Table S7: Selected non-bonding bonding interactions for **2-Zn**. **D** represents the hydrogen bond donor, **H** represents hydrogen and **A** represents the hydrogen bond acceptor.

D H···A	d(H···A) (Å)	D(D···A) (Å)	< DHA (°)
C5 H5···O3	2.560(9)	3.150(14)	121.70(55)
C1 H1···O4	2.671(10)	3.225(10)	118.90(33)
C12 H12···S2	2.919(9)	3.867(12)	162.45(31)
C17 H17···N4	2.487(8)	3.302(10)	146.32(36)

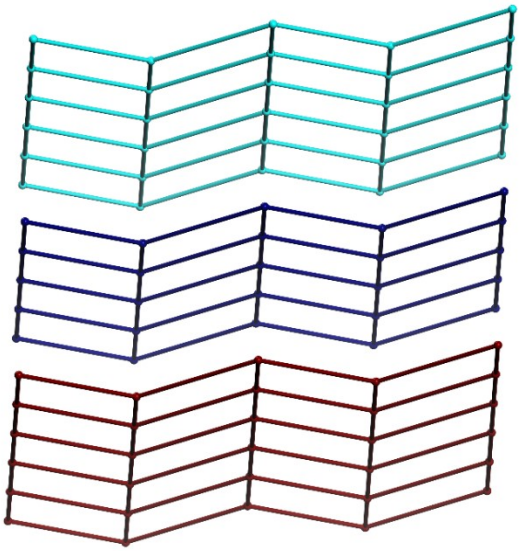

Figure S9: Representation of **2-Zn** showing the network layer with ***sql*** topology. Light blue, dark blue and maroon nets indicate the different layers**.**

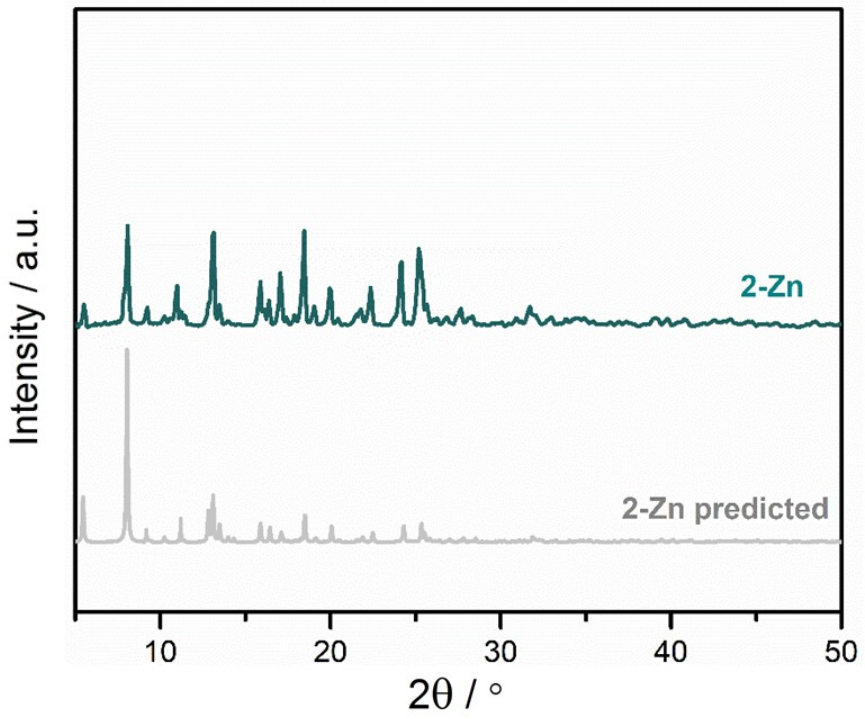

Figure S10: PXRD patterns of **2-Zn** simulated from SCXRD (grey; 298 K) and as-synthesised (green; 298 K).

Table S8: Selected bond lengths and angles for **3-Zn**.

Bond Length	Length (Å)	Bond Angle	Angle (°)
Zn1−O1	2.056(5)	O1 −Zn1− O4	158.3(2)
Zn1−O4	2.087(5)	O1− Zn1− O6	86.0(2)
Zn1−O6	2.072(8)	O1 −Zn1− O8	91.9(2)
Zn1−O8	2.061(8)	O1 −Zn1 −N5	101.5(2)
Zn1−N5	2.057(6)	O1− Zn1− Zn2	78.30(15)
Zn2−O2	2.075(5)	O2 −Zn2− O3	156.7(2)
Zn2−O3	2.055(5)	O2 −Zn2− O5	88.1(2)
Zn2−O5	2.061(8)	O2 −Zn2 −O7	86.4(2)
Zn2−O7	2.072(8)	O2− Zn2 −N1	102.1(2)
Zn2−N1	2.049(6)	O2− Zn2− Zn1	79.40(14)
Zn1−Zn2	2.950(3)	O3− Zn2− O5	88.4(2)
		O3− Zn2 −O7	88.4(2)
		O3 −Zn2− N1	101.0(2)
		O3 −Zn2− Zn1	77.28(16)
		O4− Zn1 −O6	87.2(2)
		O4 −Zn1− O8	86.5(2)
		O4 −Zn1− N5	100.1(2)
		O4 −Zn1− Zn2	80.07(15)
		O5 −Zn2 −O7	158.3(2)
		O5− Zn2− Zn1	82.7(2)
		O6 −Zn1− O8	157.2(2)
		O6 −Zn1 −N5	105.8(3)
		O6 −Zn1 −Zn2	75.9(2)
		O7 −Zn2− N1	95.1(3)
		O7 −Zn2− Zn1	75.7(2)
		O8 −Zn1 −N5	96.9(3)
		N1 −Zn2 −Zn1	170.62(17)
		N5 −Zn1 −Zn2	178.31(17)

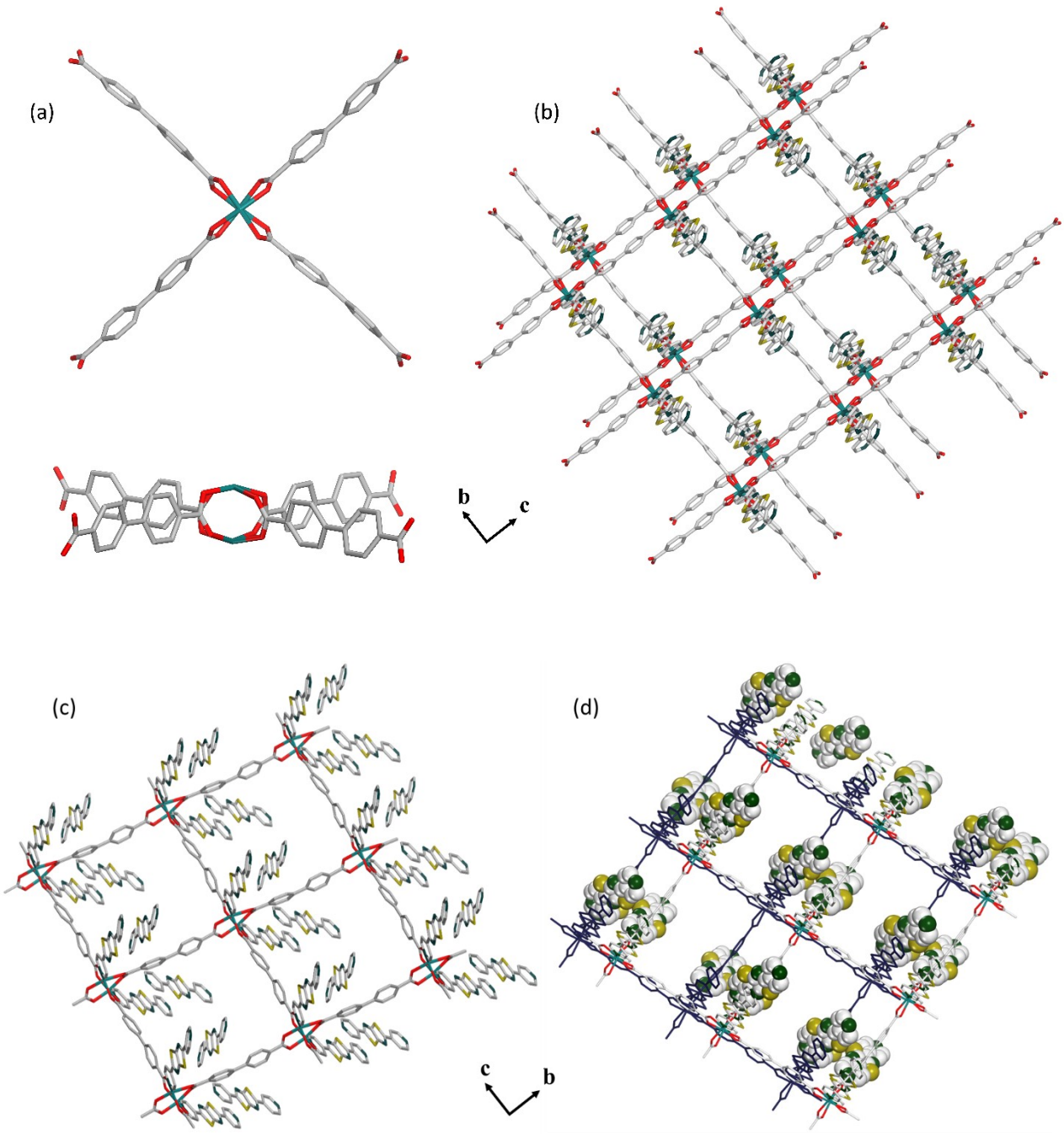

Figure S11: The crystal structure of **3-Zn**. **(a)** The Zn^{II} dimer showing the paddlewheel connectivity. **(b)** Stacking of the two-dimensional layers in **3-Zn**. **(c)** showing the uncoordinated **L** within the pores. **(d)** Uncoordinated **L** in the pores shown in CPK model. Zn – cyan, C – grey, O – red, N – blue, S – yellow (hydrogen atoms are omitted for clarity).

Table S9: Selected bond lengths and angles for **3-Zn**.

D H···A	d(H···A) (Å)	D(D···A) (Å)	< DHA (°)
C46 H11···N2	2.729(23)	3.489(24)	137.5(86)
C13 H13···N11	2.333(13)	3.166(19)	146.08(156)
C30 H30···N6	2.580(18)	3.354(21)	138.81(83)
C4 H4···N8	2.564(17)	3.507(25)	171.57(136)
C55 H55···N12	2.585(12)	3.450(15)	151.39(127)
C6 H6···N4	2.638 (14)	3.459 (20)	144.77(136)
C57 H57···S4	2.894(36)	3.725(40)	146.87(86)

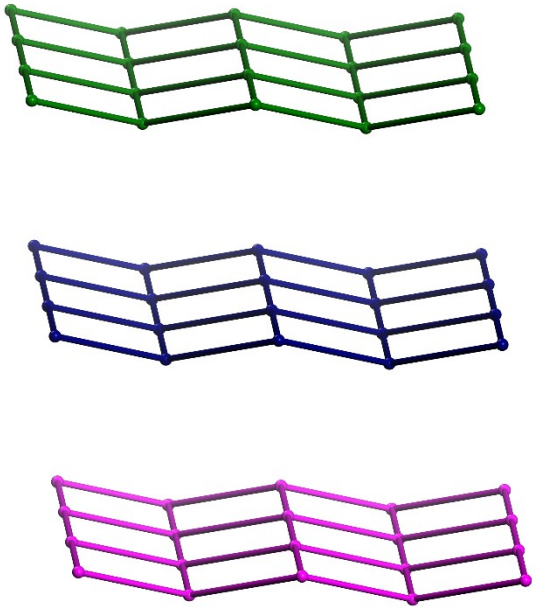

Figure S12: Representation of **3-Zn** showing the network layer with ***sql*** topology. The layers are highlighted in pink, blue and green.

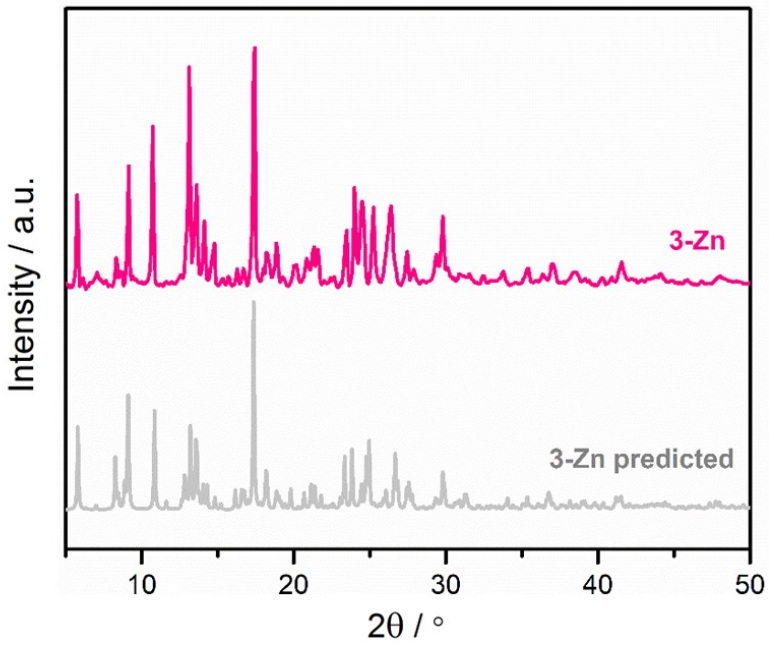

Figure S13: PXRD patterns of **3-Zn** simulated from SCXRD (grey) and as-synthesised (pink).

Physical Properties of MOFs containing L

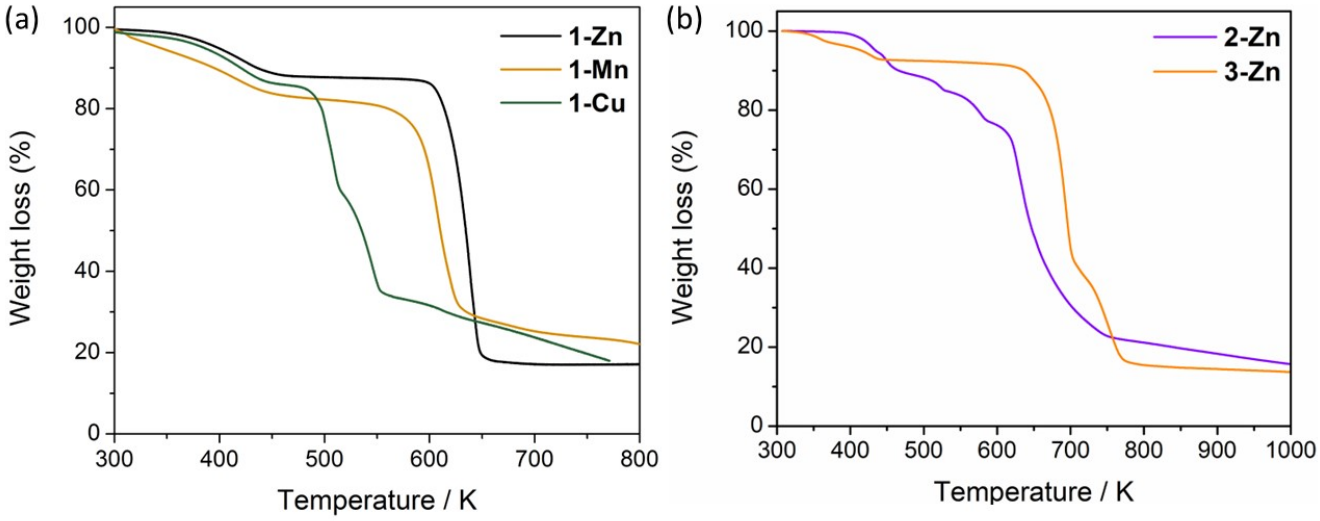

Figure S14: TGA data for **(a) 1-Zn** (black), **1-Mn** (yellow), **1-Cu** (green), **(b) 2-Zn** (purple) and **3-Zn** (orange).

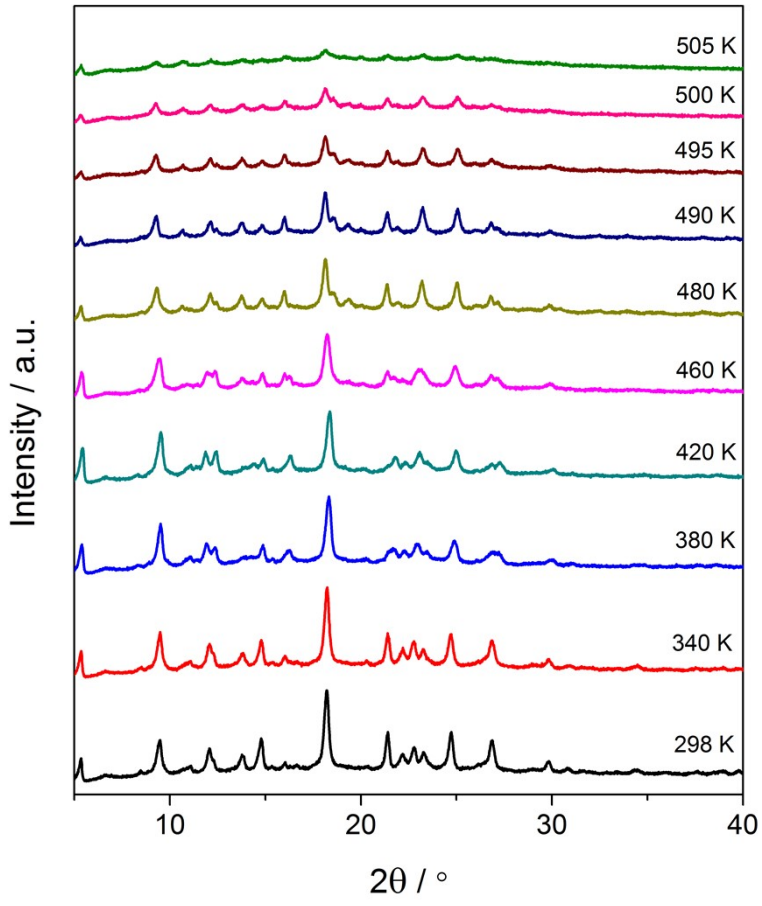

Figure S15: Variable temperature PXRD data for **1-Cu** over the range 298-505 K.

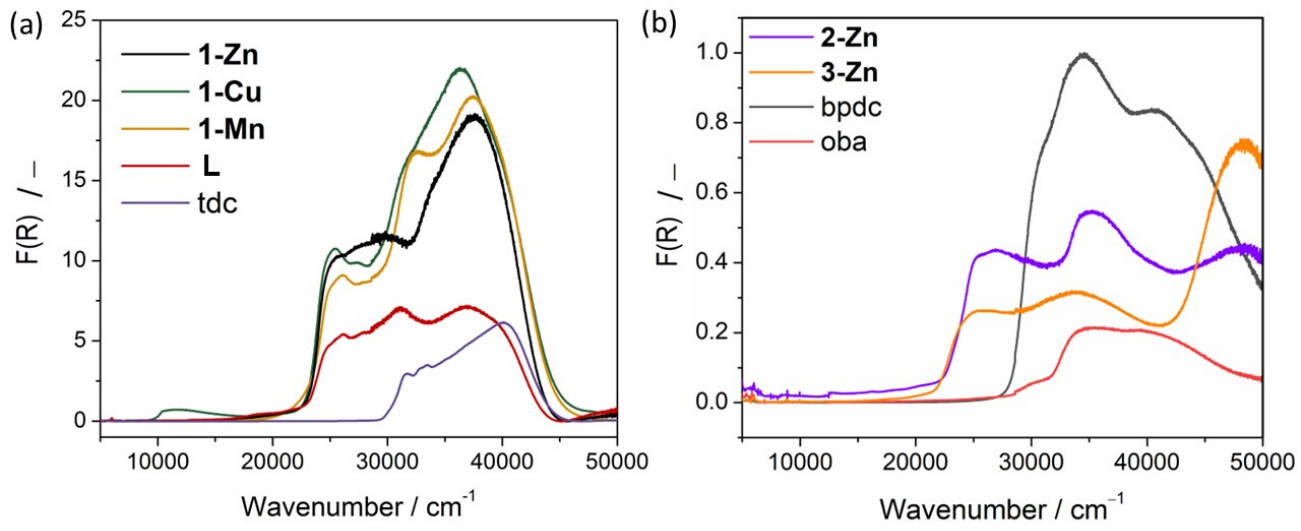

Figure S16: Solid-state UV-Vis-NIR data for **(a) 1-Zn** (black), **1-Mn** (yellow), **1-Cu** (green), **L** (red) and H_2tdc (purple), and **(b) 2-Zn** (purple), **3-Zn** (orange), H_2bpdc (black) and H_2oba (red).

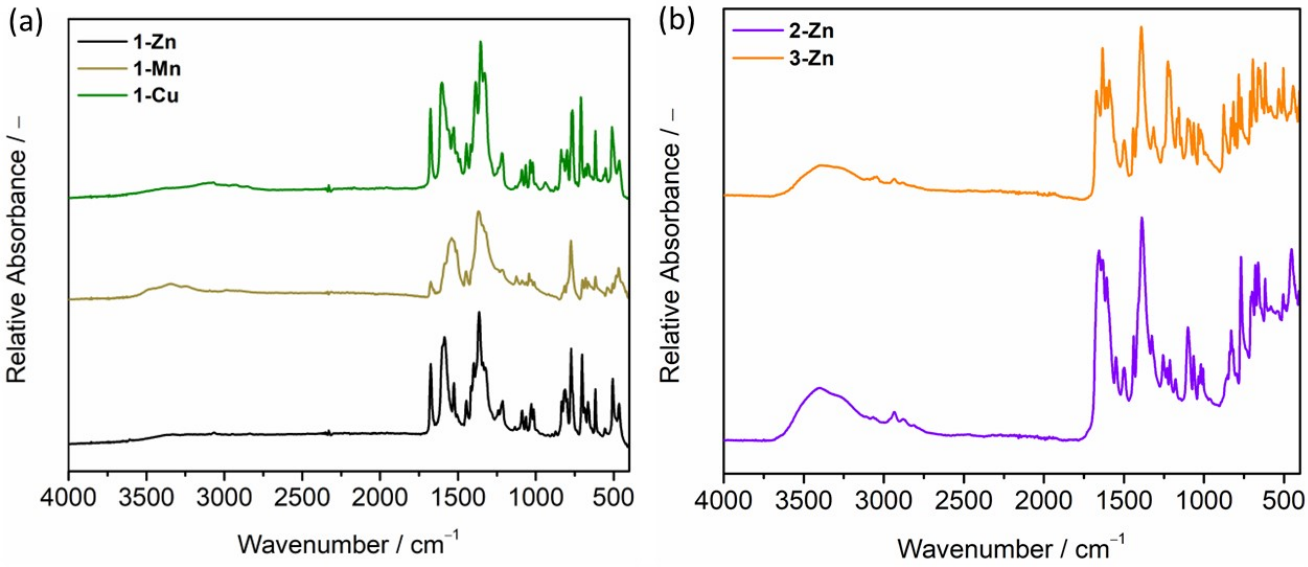

Figure S17: Solid-state FTIR data for **(a) 1-Zn** (black), **1-Mn** (yellow), **1-Cu** (green) **(b) 2-Zn** (purple) and **3-Zn** (orange).

Electronic Properties of MOFs containing L

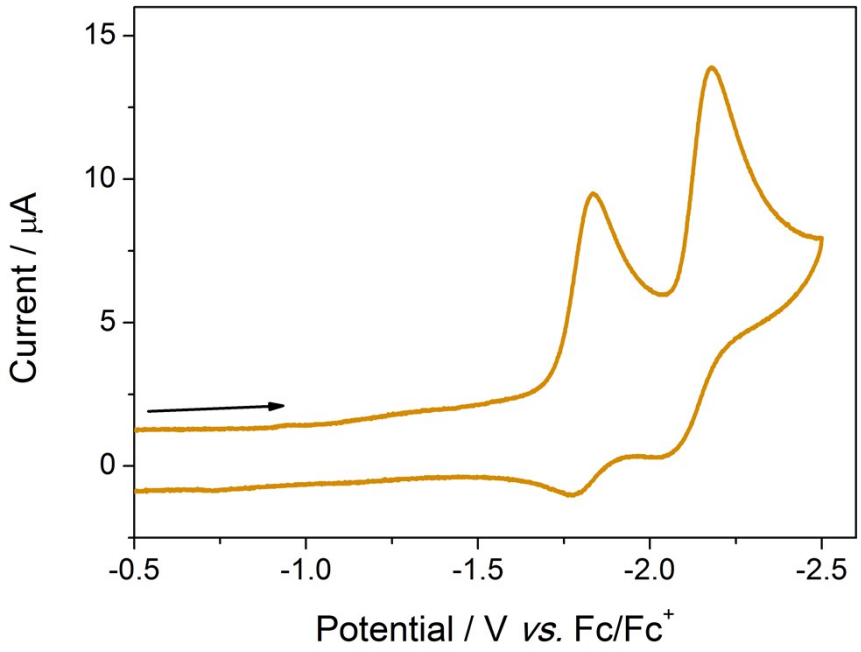

Figure S18: Solid-state CV of **1-Mn** in [*n*-Bu_4N]PF_6 (0.1 M)/acetonitrile electrolyte at a scan rate of 200 mV s^{-1}. The arrow indicates the direction of the scan.

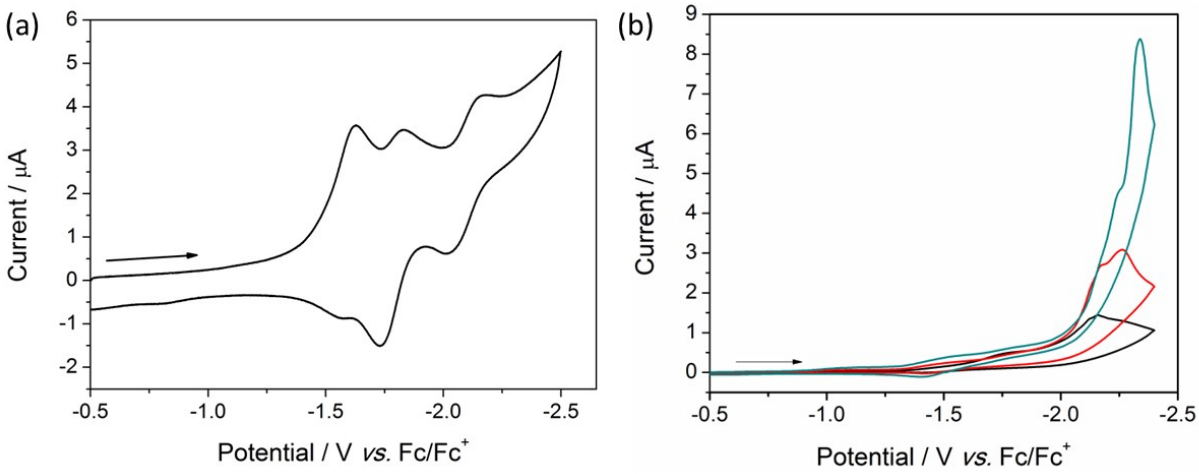

Figure S19: Solid-state CV of **(a) 1-Zn** at a scan rate of 200 mV s^{-1} and **(b) 2-Zn** at a scan rate of 25 mV s^{-1} (black), 50 mV s^{-1} (red) and 150 mV s^{-1} (green) in [*n*-Bu_4N]PF_6 (0.1 M)/acetonitrile electrolyte. The arrows indicate the directions of the forward scan.

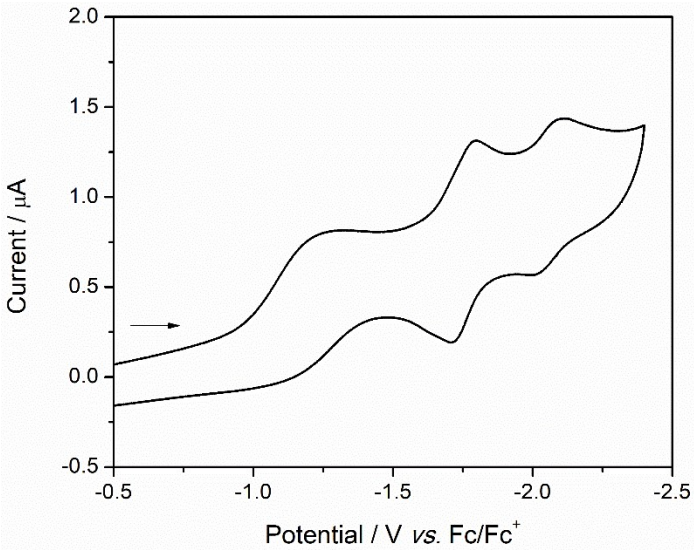

Figure S20: (a) Solution-state CV of the baseline following solid-state measurements on **2-Zn** at a scan rate of 100 mVs^{-1}. The presence of redox waves in the CV of the electrolyte solution indicate that the compound is unstable to reduction. [*n*-Bu_4N]PF_6 (0.1 M)/acetonitrile electrolyte. The arrows indicate the directions of the forward scan.

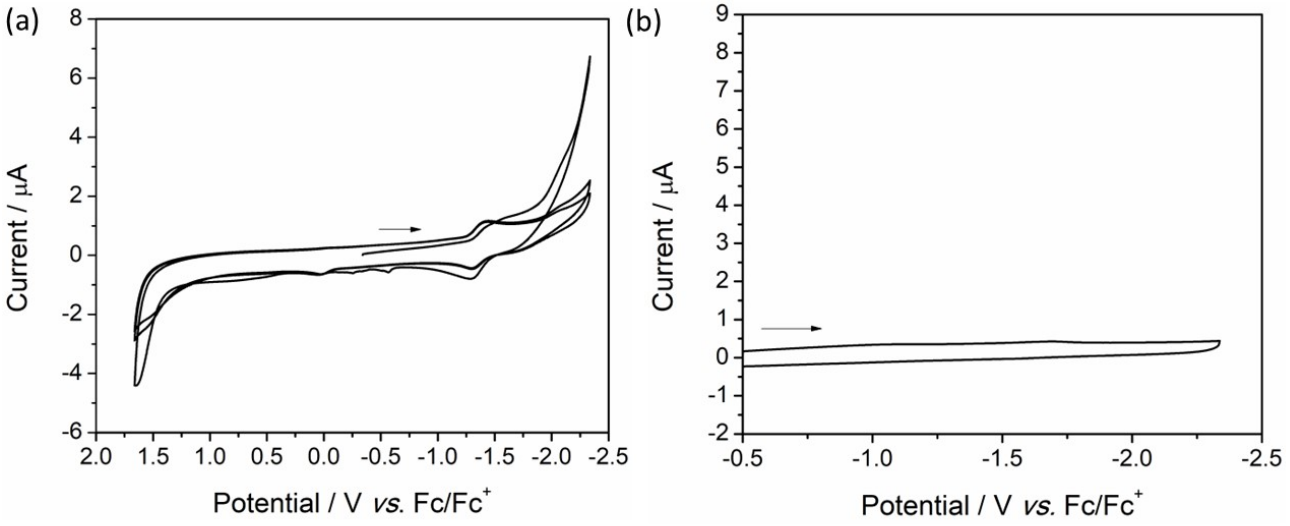

Figure S21: (a) Solid-state CV cycling of **3-Zn** at a scan rate of 100 mVs^{-1}. **(b)** solution state CV of the baseline following solid-state measurements on **3-Zn**. [*n*-Bu_4N]PF_6 (0.1 M)/acetonitrile electrolyte. The arrows indicate the directions of the forward scan.

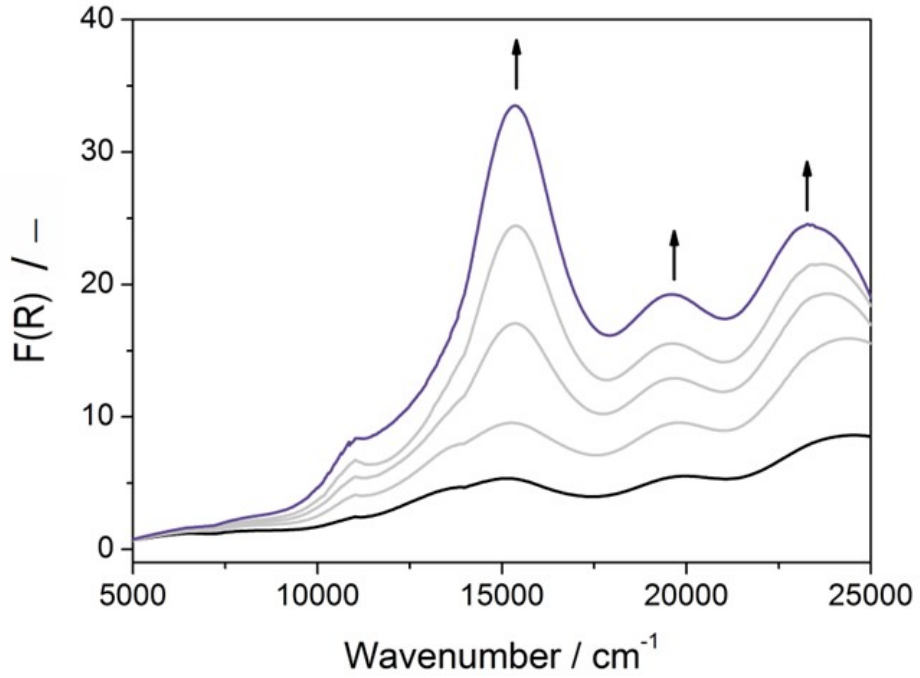

Figure S22: (a) Solid-state SEC on **1-Cu** upon application of a potential at −2.0 V *vs.* Ag/Ag^+. [*n*-Bu_4N]PF_6 (0.1 M)/acetonitrile electrolyte. The arrows indicate spectral progression.

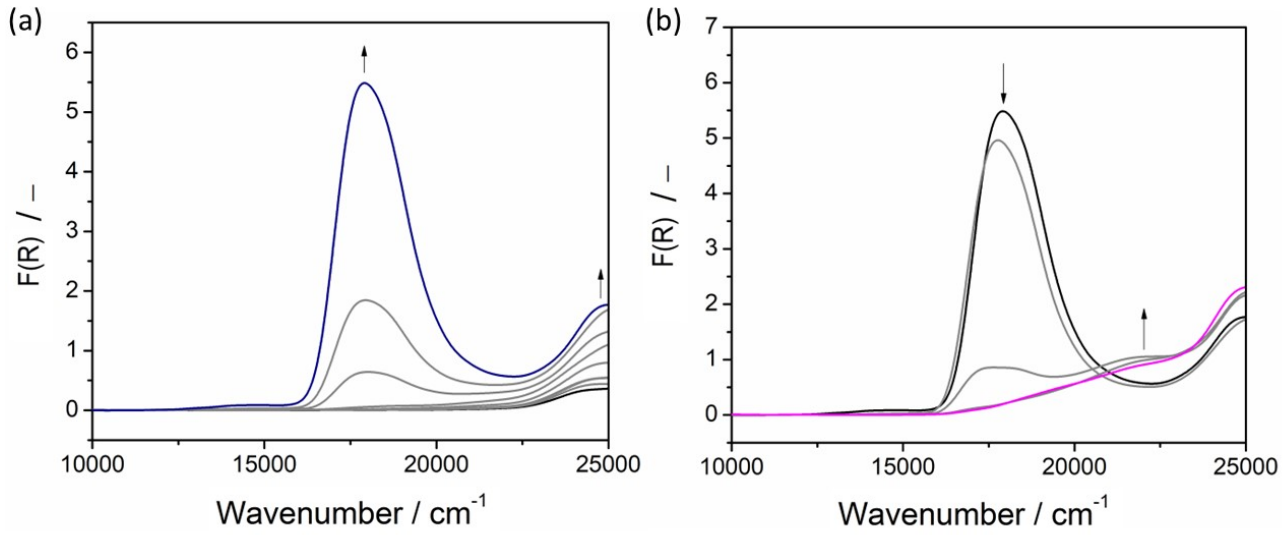

Figure S23: Solid-state SEC of **2-Zn** upon applying a stepwise potential from **(a)** 0.0 V to −2.0 V *vs.* Ag/Ag^+ and **(b)** −2.0 V to 0.0 *vs.* Ag/Ag^+. [*n*-Bu_4N]PF_6 (0.1 M)/acetonitrile electrolyte. The arrows indicate spectral progression.

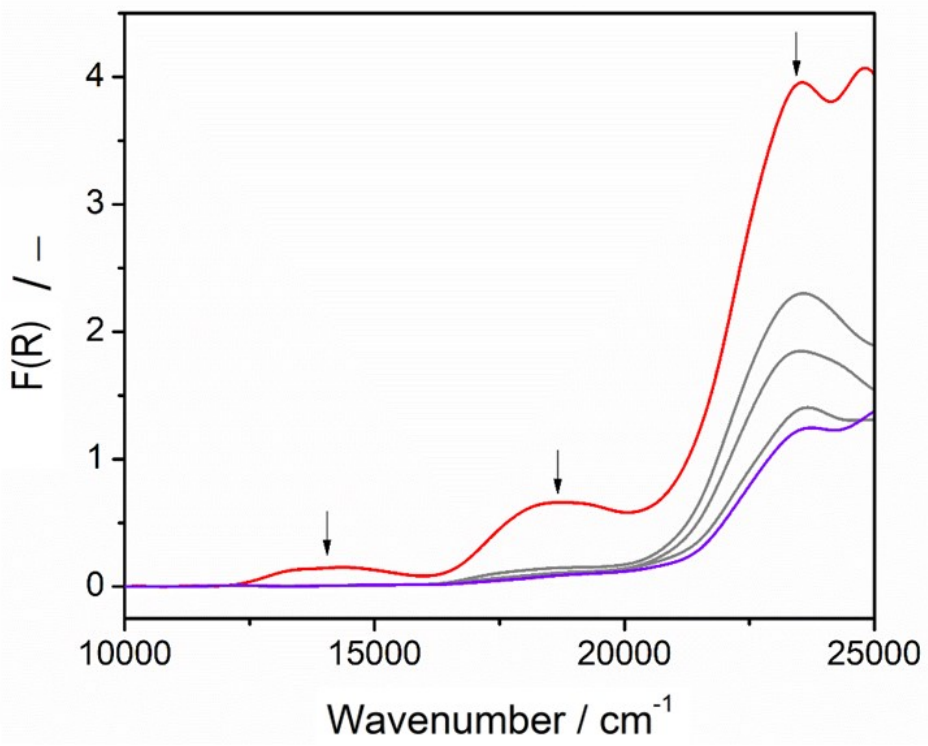

Figure S24: (a) Solid-state SEC on **3-Zn** upon application of a stepwise potential from −2.0 V to 0.0 *vs.* Ag/Ag^+. Recovery of the initial spectrum suggests that **3-Zn** maintains its integrity. [*n*-Bu_4N]PF_6 (0.1 M)/acetonitrile electrolyte. The arrows indicate spectral progression.

References

1. S. Hisamatsu, H. Masu, I. Azumaya, M. Takahashi, K. Kishikawa and S. Kohmoto, *Cryst. Growth Des.*, 2011, **11**, 5387-5395.
2. A. C. Larson and R. B. V. Dreele, *General structure analysis system (GSAS)*, Los Alamos National Laboratory Report LAUR 86-748, 2000.
3. B. H. Toby, *J. Appl. Crystallogr.*, 2001, **34**, 210-213.
4. C. F. Macrae, P. R. Edgington, P. McCabe, E. Pidcock, G. P. Shields, R. Taylor, M. Towler and J. van De Streek, *J. Appl. Crystallogr.*, 2006, **39**, 453-457.
5. P. M. Usov, C. Fabian and D. M. D'Alessandro, *Chem. Commun.*, 2012, **48**, 3945-3947.
6. Agilent (2014). *CrysAlis PRO*. Agilent Technologies Ltd, Yarnton, Oxfordshire, England..
7. L. J. Farrugia, *J. Appl. Crystallogr.*, 1999, **32**, 837-838.
8. O. V. Dolomanov, L. J. Bourhis, R. J. Gildea, J. A. K. Howard and H. Puschmann, *J. Appl. Crystallogr.*, 2009, **42**, 339-341.
9. G. M. Sheldrick, *SHELX97 programs for crystal strucure analysis*, University of Göttingen. Institüt für Anorganische Chemie der Universität, Tammanstrasse 4, D-3400 Göttingen, Germany, 1998.
10. A. L. Spek, *J. Appl. Crystallogr.*, 2003, **36**, 7-13.
11. L. J. Barbour, *J. Supramol. Chem.*, 2001, **1**, 189-191.
12. Bruker, 1999, *SAINT+*, version 6.02, Bruker AXS Inc., Madison, Wisconsin, USA.
13. G.M. Sheldrick, 1995. *XPREP*. Version 5.1. Siemens Analytical X.
14. G. M. Sheldrick, *SHELXTL™ Reference Manual: version 5.1,* Bruker AXS, Madison, WI, **1997**.
15. G. M. Sheldrick, *Acta Crystallogr C Struct Chem*, 2015, **71**, 3-8.